



A discussion on the formation mechanism of tungsten carbides during mechanical milling of CaWO_4 –Mg–C mixtures



Hossein Yavari Mehrabani, Abolfazl Babakhani*, Jalil Vahdati-Khaki

Department of Materials Science and Metallurgical Engineering, Engineering Faculty, Ferdowsi University of Mashhad, Mashhad, Islamic Republic of Iran

ARTICLE INFO

Article history:

Received 22 May 2018

Received in revised form

3 December 2018

Accepted 4 December 2018

Available online 8 December 2018

Keywords:

Mechanically-induced self-propagating

reaction

Scheelite

Tungsten carbide

Planetary ball mill

ABSTRACT

Synthesis mechanism of tungsten carbides via mechanically-induced self-propagating reaction (MSR) was investigated. Scheelite (CaWO_4) is the main ore of tungsten and was used as precursor of tungsten in this study. To investigate the effect of magnesium and carbon contents on the milling products various mixtures were prepared according to the following equation: $\text{CaWO}_4 + x \text{Mg} + (4 - x) \text{C} = \text{WC} + x \text{MgO} + (3 - x) \text{CO}_{(g)} + \text{CaO}$. The value of x was varied from 0.5 to 3. It was seen that the reaction is gradual when $x \leq 2$ while the reaction occurred in MSR mode at higher x values. CO gas was detected in vial for samples in MSR mode that was due to participation of carbon in reduction reaction of scheelite. Therefore W_2C phase was formed because of carbon deficiency. WC was not formed because of high reaction temperature and carbon deficiency. In the second group of experiments milling of $\text{CaWO}_4 - 3 \text{Mg} - (1 + y) \text{C}$ mixtures were investigated. The elimination of carbon deficiency was the aim of these experiments. It was seen that metallic tungsten was converted to W_2C . Addition of more carbon lead to the formation of WC at $y = 0.8 - 1$. WC disappeared by addition of more carbon due to decrease of adiabatic temperature and interruption of atomic diffusion.

© 2018 Elsevier B.V. All rights reserved.

1. Introduction

Recent development of nanostructure materials suggest that the nano-structured cemented tungsten carbides can introduce a group of materials with significantly improved mechanical properties [1]. There are two challenges for production of these materials. The first is the synthesis of tungsten carbide nano-particles and the second is the consolidation method. W [2], WO_3 [3] and WCl_6 [4,5] were main precursors in the literature for the synthesis of nano-sized tungsten carbide. These materials are intermediate or final products of multi-step hydro- and/or pyrometallurgical processing of scheelite (CaWO_4). Scheelite and wolframite [$\text{Fe}(\text{Mn})\text{WO}_4$] are the main primary resources of tungsten that are enriched by physical beneficiation to obtain concentrate assaying around 60% WO_3 [6,7]. Thus, direct production of tungsten carbide from scheelite can be eco-friendly. Dry autoclaving is one the methods for synthesis of various refractory compounds [8,9]. Singh and Pandey [10] have used this method for production of tungsten carbide from scheelite

by heating of CaWO_4 –Mg–C mixture in an autoclave at 650 °C for 20 h. The final product was nano-sized tungsten carbide (WC). Similar research has been done by theme using wolframite as precursor [11]. The other method is the carbothermic reduction of scheelite. Polini et al. [12–14] have investigated the reaction mechanism of activated scheelite-carbon mixtures at different temperatures (1100–1400 °C). They have observed the formation of Ca_3WO_6 , W and W_2C as intermediate phases. Similar results have been reported by Singh and Pandey [15]. Both of these methods need high temperatures and/or long time activation (24–150 h). Thus, a fast and low temperature method can be advantageous. One of the suggested processes for synthesis of nano-particles is mechanically-induced self-propagating reaction (MSR). In this method a self-sustaining reaction is initiated in a highly exothermic powder mixture by mechanical milling. This method can be characterized by its short processing time.

The synthesis of tungsten carbide by MSR process have been investigated by several researchers. Most of them have used WO_3 as precursor for the synthesis of tungsten carbide. El-Eskandarani [3] reported the formation of metallic tungsten by milling of WO_3 , Mg and graphite mixture after 24 h. Conversion of metallic tungsten to tungsten carbide occurred after 48 h milling. Similar experiment was carried out by Pallone et al. [16] on the WO_3 , Al and carbon

* Corresponding author. Department of Materials Science and Metallurgical Engineering, Engineering Faculty, Ferdowsi University of Mashhad, Azadi square, Mashhad, 9177948974, Islamic Republic of Iran.

E-mail address: babakhani.fum@gmail.com (A. Babakhani).

mixture with this difference that amorphous carbon was used instead of graphite and hence the formation of metallic tungsten occurred after 45 min. Graphite has a lubricating property and prolongs the milling process. In addition, formation of intermediate phases during milling process were observed by Pallone while El-Eskandarani could not detect any intermediate phase in the synthesis process of tungsten carbide. Several papers were published by Sakaki et al. [17–21] about effect of the reactants content on the products of MSR process but these researches were limited to the identification of final phases without any discussion about the reactions sequences.

Unlike the above mentioned researches, scheelite (CaWO_4) has been used as precursor (instead of WO_3) for the synthesis of tungsten carbide in the present study. As it is mentioned earlier, the synthesis of tungsten carbide via MSR process includes two main steps. The first is formation of metallic tungsten. This step has been investigated by authors and the results have been published elsewhere [22]. The second step is formation of tungsten carbide by reaction of metallic tungsten and carbon. The aim of the present study is to investigate the effect of reactants contents on the MSR products.

2. Materials and methods

Analytical grade of hydrated sodium tungstate ($\text{Na}_2\text{WO}_4 \cdot 2\text{H}_2\text{O}$) and hydrated calcium chloride ($\text{CaCl}_2 \cdot 2\text{H}_2\text{O}$) were used to obtain synthetic scheelite. Equimolar quantities of $\text{Na}_2\text{WO}_4 \cdot 2\text{H}_2\text{O}$ and $\text{CaCl}_2 \cdot 2\text{H}_2\text{O}$ were dissolved in distilled water kept at 60°C in separate beakers. CaWO_4 was precipitated according to reaction 1 by gradual addition of CaCl_2 solution into the beaker containing Na_2WO_4 solution at constant stirring speed. The synthesized CaWO_4 was allowed to settle and then supernatant was decanted. The precipitate was washed with distilled water repeatedly to remove NaCl , the by product that was formed, as well as the unreacted Na_2WO_4 and CaCl_2 . The synthesized scheelite was dried for 5 h at 140°C and was finally well ground to break up any agglomerate.



Fig. 1 shows the synthesis of scheelite schematically. It can be seen that Ca^{2+} and $(\text{WO}_4)^{2-}$ ions make bonds and insoluble scheelite forms immediately after mixing the solutions. Synthesized scheelite was characterized by X-ray diffractometry and Raman spectroscopy to ensure the similarity with natural crystal of scheelite. Additionally the particle size and morphology of synthesized scheelite was investigated by particle size distribution analysis and field-emission electron microscopy.

The target of this research is to investigate the reaction

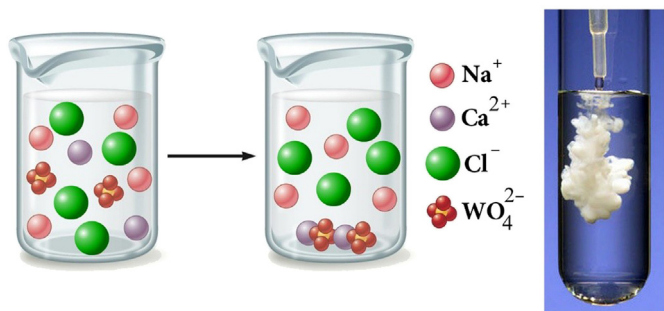


Fig. 1. Synthesis and precipitation of CaWO_4 immediately after mixing of solutions containing Ca^{2+} and $(\text{WO}_4)^{2-}$ ions.

mechanism of scheelite–magnesium–carbon mixtures during mechanical milling based on temperature monitoring. The main method for recognition of the events during the process is to measure the temperature of vial. Thus it is necessary to use a sensitive and accurate temperature data logger, whereas commercial temperature monitoring systems use types of thermocouples that have problems such as delay in signal transmission and low sensing resolution. Therefore the temperature of vial was monitored using a self-designed temperature data logger. DS18B20 digital temperature sensor was used in this data logger. The operating temperature range of this sensor was -55°C to $+125^\circ\text{C}$. The resolution of the sensor was set at 0.125°C . The accuracy of the sensor is about 0.1°C in the range of 25 – 40°C . The system measures and saves the temperature every 375 ms. The detailed information about the accuracy and possible systematic error of sensor has been mentioned in the data sheet [23]. The thickness of the wall in the sensor installation spot was just 1 mm. The data was transmitted to the stationary receiver which send them to the MATLAB R2012a software through a serial interface. ATmega16 microcontroller was used in the data logger and data receiver. Programming of microcontrollers were carried out using Atmel studio software. It should be noted that the reported graphs were smoothed in MATLAB software.

Two sets of experiments were carried out in the present study. In the first group the effect of magnesium and carbon contents on the reaction mechanism during mechanical milling were studied. Therefore, the equation given below was considered as probable reaction:



Where the values of x were varied as 0.5, 1, 1.5, 2, 2.5, 2.9 and 3.

In the second group of experiments, the effect of carbon content on the reaction was investigated. Accordingly, various mixtures of $\text{CaWO}_4 - 3 \text{Mg} - (1 + y) \text{C}$ were milled until immediately after observing the abrupt temperature increase. The value of y varied from 0 to 2.8.

For milling experiments, powders were loaded in a 200 ml hardened steel vial. The mass of the samples were kept constant (4.12 g) in all experiments. Three sizes of hardened steel balls (6, 8 and 10 mm) were used in the process with ball to powder ratio of 30:1. The vial:supporting disk rotation velocity ratio was 2:1 and the supporting disk speed was 250 rpm. After interruption of milling, the gases generated during the process, CO/CO_2 , were evaluated by MQ-7 semiconductor gas sensor. The detailed information about the accuracy and operation mechanism of this sensor has been mentioned in the data sheet [24].

Samples were analyzed by X-ray diffraction (EXPLORER GNR analytical instrument group) equipped with a plane monochromator using $\text{Cu K}\alpha$ radiation ($\lambda = 1.5418 \text{ \AA}$). Diffraction patterns were acquired using a count time of 1 s per 0.02° step. The obtained diffractograms were matched with ICDD standard cards using X'pert High Score software and the details of the cards are given in Table 1. Scheelite powder was imaged using a field emission scanning electron microscope (FESEM) (MIRA3 TESCAN). Thermodynamic calculations were performed using the FactSage 6.1

Table 1
ICDD standard cards with the compounds found in XRD results.

Compound	ICDD card	Compound	ICDD card
CaWO_4	01-072-0257	Mg	01-089-5003
Ca_2MgWO_6	00-048-0108	MgO	01-079-0612
WO_{3-x}	00-053-0434	WC	01-079-0097
W	01-089-3728	W_2C	00-035-0776

thermochemical software.

3. Thermodynamic aspects

It should be mentioned that the thermodynamic calculations are incapable for precise prediction of non-equilibrium processes such as MSR but concerning them can be beneficial to interpret the events. Two groups of reactions can occur in CaWO_4 –Mg–C mixtures. The first group is the reduction of CaWO_4 to metallic tungsten that can be considered as below reactions:

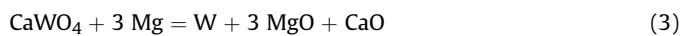


Table 2 shows the thermodynamic characteristics in standard conditions belonging to these reactions. The negative value of ΔG for magnesiothermic reduction reaction indicates that the thermodynamic conditions are provided for proceeding of this reaction in the forward direction. Additionally this reaction is highly exothermic and release a great deal of heat that raise the adiabatic temperature to about 3533 K. In return, the carbothermic reduction reaction is highly endothermic and cannot occur in standard conditions due to its positive ΔG . It should be noted that according to the Merzhanov criterion, if the $T_{ad} > 1800$ K, the reactions can occur in a self-propagating high temperature synthesis (SHS) mode [25]. Herein, the calculated adiabatic temperatures of magnesiothermic reduction reaction is higher than 1800 K and theoretically it can occur in SHS mode. Fig. 2 shows the ΔG -T diagrams of these reactions. As it can be seen the magnesiothermic reaction can lead to the formation of metallic tungsten in all temperatures because of negative values of ΔG while the carbothermic reaction can occur just in temperatures higher than ~ 1300 K. Additionally in a system with simultaneous presence of magnesium and carbon the

Table 2
Thermodynamic information of possible reactions in CaWO_4 –Mg–C system.

Reaction number	ΔG (kJ/mol)	ΔH (kJ/mol)	T_{ad} (K)
3	–775	–820	3533
4	501	656	–
5	–40	–40	1161
6	–14	–13	602
7	–27	–26	899

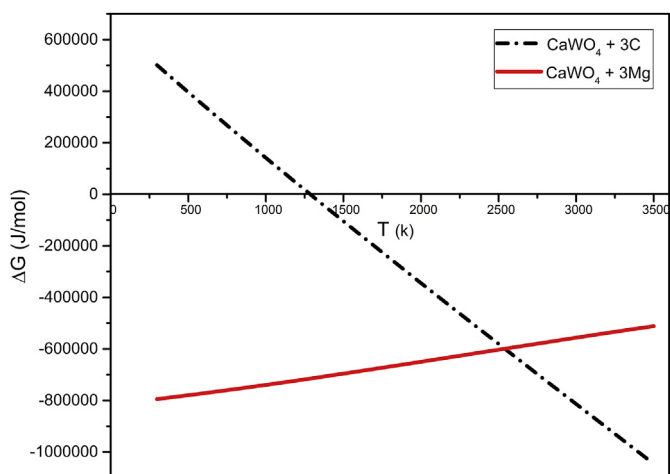


Fig. 2. ΔG -T plots for magnesiothermic and carbothermic reduction reactions.

carbothermic reaction can be activated in temperatures higher than ~ 2500 K due to more negative values of ΔG .

The second group of reactions in CaWO_4 –Mg–C system relates to the formation of tungsten carbides. These reactions can be considered as:



The thermodynamic characteristics of these reactions are mentioned in Table 2. It is seen that these reactions are exothermic and they can occur in standard conditions because of their negative values of ΔG . The adiabatic temperature of these reactions are lower than 1800 K. Thus these reactions cannot occur in SHS mode based on Merzhanov criterion. Fig. 3 shows the ΔG -T plots of these reactions. In temperatures higher than 1500 K the formation reaction of W_2C can occur due to more negative values of ΔG while in temperatures lower than 1500 K the formation of WC is the preferred reaction. In addition the conversion reaction of W_2C to WC can take place in temperatures lower than 1500 K.

Fig. 4 shows ΔG -x, ΔH -x and T_{ad} -x plots for reaction 2. It can be seen that calculated adiabatic temperature increases by increasing the x value. Maximum adiabatic temperature was attained at $x = 3$. In this mixture, it was assumed that all of the sheelite is reduced by magnesiothermic reaction and WC forms by subsequent reaction of tungsten and carbon. Both the reactions are exothermic and therefore highest adiabatic temperature is attained in this mixture. It is assumed that the CaWO_4 can be reduced by magnesium and carbon simultaneously in mixtures with lower x value. In other word the evolved heat of CaWO_4 and Mg reaction can activate the endothermic reaction of CaWO_4 and carbon. Therefore the adiabatic temperature decreases by decreasing x value. As it can be seen in Fig. 4 the reactions can occur in a self-propagating mode for x values more than ~ 2 according to the Merzhanov criterion. The adiabatic temperature cannot be calculated for x values lower than 1.3 because the reactions taking place at these x values are inherently endothermic. For a mixture containing 4 mol of carbon ($x=0$), ΔG has a large positive value (480 kJ/mol). This positive ΔG shows that the reaction cannot occur from the thermodynamic view point. As Mg increases, ΔG values of mixtures decrease and finally become zero at $x = 1.1$ and find negative values thereafter which is

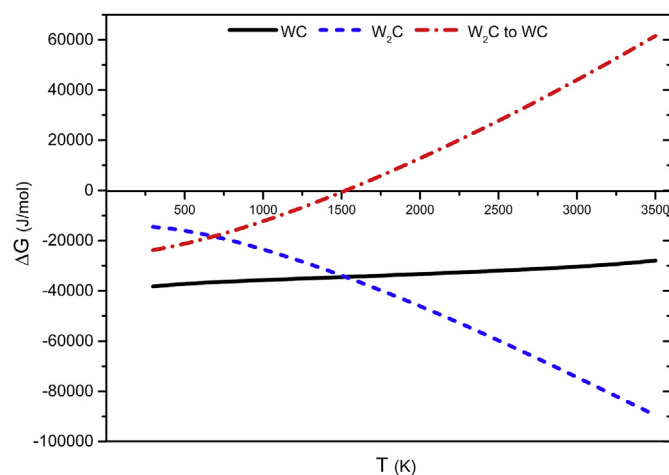


Fig. 3. ΔG -T plots of tungsten carbides formation reactions.

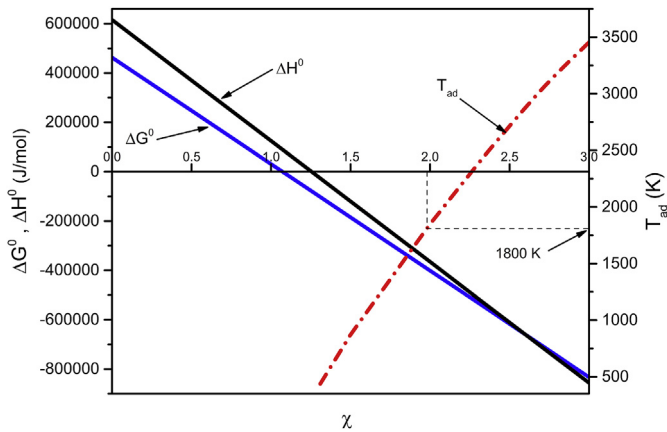


Fig. 4. ΔG° , ΔH° - x and T_{ad} - x plots for reaction 2.

thermodynamically favorable.

4. Results and discussion

4.1. Characterization of synthesized scheelite

We have drawn a comparison between the synthesized scheelite and the natural sample that is kept in the University of Arizona Mineral Museum [26] by Raman spectroscopy and X-Ray diffractometry. The detailed results have been reported elsewhere [22]. The obtained patterns of XRD and Raman spectroscopy have shown a good similarity between two samples. Additionally, no excess or unidentified peaks were seen in the patterns other than those that represent pure scheelite. Fig. 5 shows the particle size distribution and FESEM micrograph of synthesized scheelite. As it can be seen the particles have spherical morphology with size distribution lower than 1000 nm.

4.2. Milling of CaWO_4 -Mg-C mixtures

Fig. 6 represents the time dependent temperature variations of the outer wall of milling vial obtained by temperature monitoring system. Plot (a) in Fig. 6 represents a gradual trend of temperature variations for samples with $x \leq 2$. This temperature variations can be interpreted as gradual mode of reaction during mechanical milling. There are two main mechanisms for explaining the temperature increase in these samples. The first is the conversion of mechanical energy to heat. It has been reported that more than 90% of mechanical energy imparted to the powders is transformed into heat [27]. Additionally the collision of balls to the surroundings (wall, powder particles and other balls) increase the overall temperature of system due to local temperature pulses [28–30]. Also investigations has revealed that friction has important role in temperature increase during milling [31]. The second mechanism of temperature increase is the release of heat by progress of gradual exothermic reaction. This mechanism has been reported by L. Takcas [32]. Based on calculations (Fig. 4) the reaction can progress in SHS mode when $T_{ad} > 1800$ K. The calculated adiabatic temperature at $x = 2$ is more than 1800 K, while the temperature variations of the vial during milling represent a gradual process. This is due to differences of MSR and SHS processes. In SHS systems, the reacting particles are in physical contact completely and the reaction propagates through a wave along the entire compact. While in MSR mode, powder particles are randomly distributed all over the vial space. Deidda et al. [33,34] photographed the collision of a ball to powder particles in a transparent vial. He observed small sparks

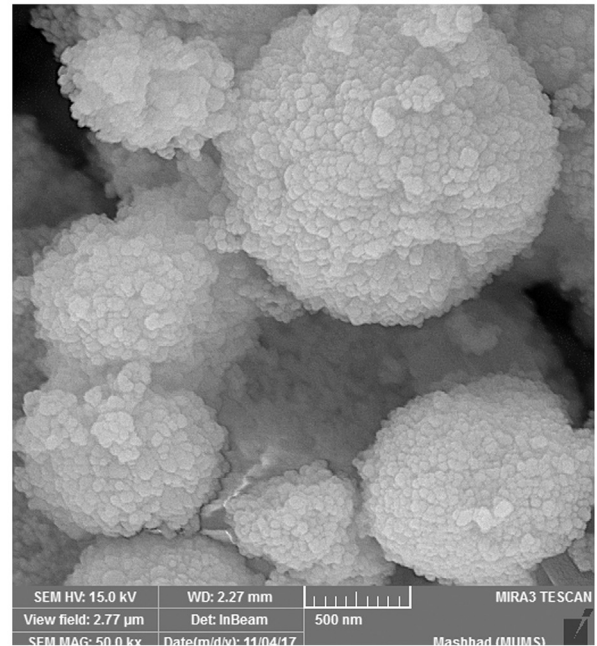


Fig. 5. FESEM and PSD analysis of synthesized scheelite.

that extinguished rapidly. This means the occurrence of reaction in collision sites. However, this local reactions cannot make a propagating wave to ignite the entire powder. Similar events can occur in the present study. Fig. 7 shows the collision moment schematically. It can be seen that the collision leads to the exothermic reaction between two particles (Fig. 7a). The released heat (Q) increase the temperature of adjacent particles. In systems containing lower diluent contents (carbon) the released heat can provide needed energy for occurrence of reaction between secondary particles (Fig. 7c). Consecutive occurrence of this event makes an ignition wave that propagate along the entire vial. For systems with lower volume fraction of reactants (or higher volume fraction of diluents like carbon in the present study) the released heat is absorbed by diluent particles that surrounded the reactants and thus the temperature of particles do not reach to the ignition temperature and hence the reaction does not occur in MSR mode (Fig. 7b).

According to Fig. 6, there is an abrupt temperature increase for $x > 2$ that represents a highly exothermic reaction during mechanical milling. It can be seen also in Fig. 8 that the ignition time decreases by increasing magnesium content (or x value) in the

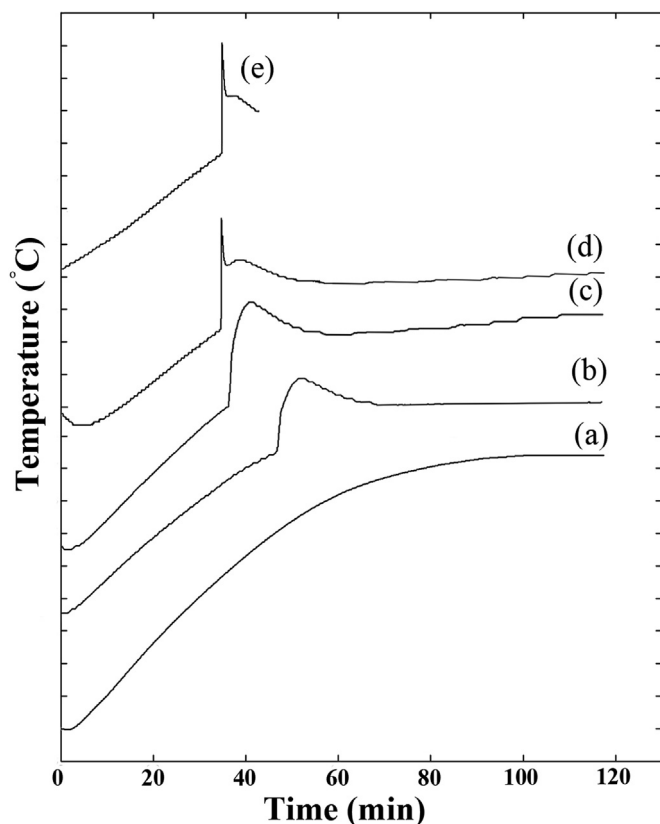


Fig. 6. Time dependent temperature variations of the milling vial for various samples. The tick marks on the temperature scale are 1 °C from each other. (a) Temperature variations pattern for samples with gradual reaction ($x \leq 2$) (b) $x = 2.5$ (c) $x = 2.9$ (d) $x = 3$ (e) $x = 3$ milled until SHS observation.

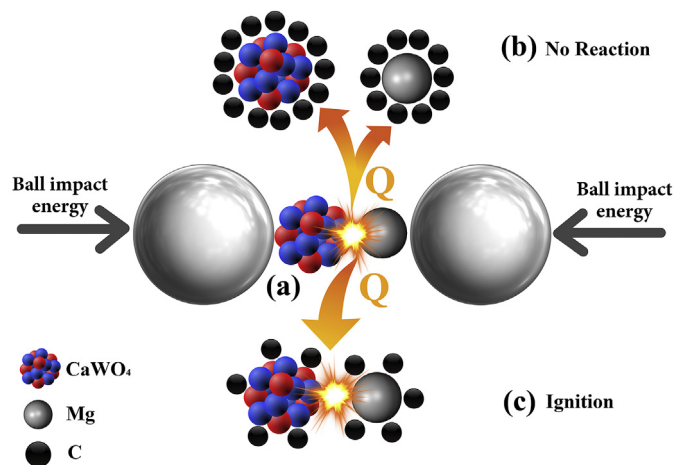


Fig. 7. Schematic representation of the collision moment (a) release of heat due to reaction between two particles (b) systems containing higher volume fraction of carbon with no reaction (c) systems containing higher volume fraction of carbon.

mixture. This is due to change in the fraction of brittle and soft reactants that affect mixing efficiency process. Although comminution takes place faster in powder mixtures with brittle components, the ignition time is longer due to lower mixing ability in these systems. On the other hand, the mixing takes place faster in the mixtures containing soft components like metals but the continuous fracturing-welding of particles can increase the ignition

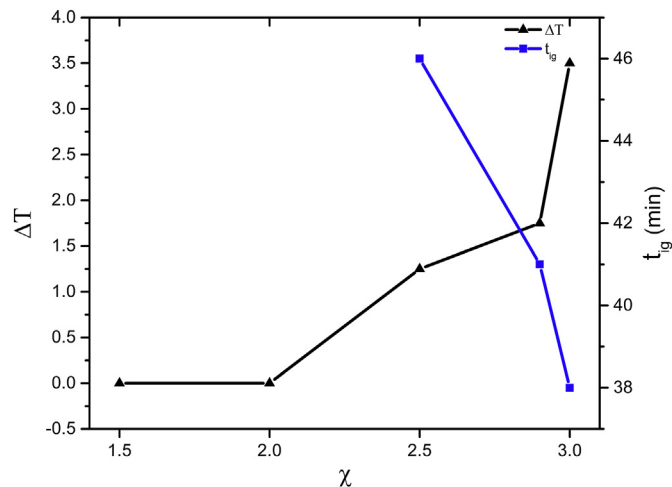


Fig. 8. Variations of t_{ig} and ΔT of ignition by x value.

time in such systems. The mixing takes place more efficient in the mixtures containing brittle and soft components simultaneously and as a result the system reaches to the activated state in shorter time [30,32]. In the present study decrease of x value means decrease in the magnesium content (soft substance) and increase of carbon and scheelite (hard substance). Therefore the ignition time increases by declining x values due to increase in the volume fraction of brittle components in the mixtures.

Fig. 8 shows the variations of ΔT of ignition by x value. It is seen that ΔT of ignition decreases by decreasing magnesium content (replacement of magnesium by carbon). Maximum ΔT is reached at $x = 3$. As it is mentioned before the reaction of scheelite and carbon is highly endothermic and as a result it cannot occur in the self-propagating mode. Therefore the first significant reaction in the process is the MSR reaction between scheelite and magnesium. By decreasing magnesium content, the released heat of MSR reaction decreases due to off-stoichiometric mixture of scheelite and magnesium. Additionally, Table 3 shows CO evolution in the samples with MSR reaction. The CO gas is the end product of the reaction between scheelite and carbon. Thus a fraction of MSR heat is consumed for progress of carbothermic reduction. It should be noted that a portion of MSR heat is absorbed by carbon and extra scheelite to reach the carbothermic reaction temperature. This effect is considered in the adiabatic calculations. As a result the ΔT of ignition decreases by decreasing x value.

There is a secondary temperature raise immediately after ignition peak in samples with MSR reaction. It can be seen also in Fig. 6 there is a temperature drop between MSR and the secondary peak at $x = 3$. In sample milled until ignition observation, the temperature variations after the temperature drop appeared as a fairly horizontal line for a few minutes and eventually dropped to the ambient temperature. We have to know the heat sources to

Table 3
Reaction mode and CO gas evolution at various x values.

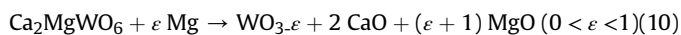
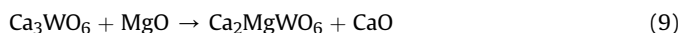
x value	Reaction mode	CO gas
0.5	Gradual	-
1	Gradual	-
1.5	Gradual	-
2	Gradual	-
2.5	MSR	+
2.9	MSR	+
3	MSR	+

interpret the temperature behavior of samples during mechanical milling. As mentioned before one of the heat sources in the milling process is the collisions and friction of balls. It is clear that this heat generation source is deactivated, when the ball mill is turned off. The other heat generation source is the highly exothermic reaction that was activated by mechanical milling. It is mentioned earlier that abrupt temperature increase is the indication for this exothermic reaction. The third source of heat generation in the process is gradual reaction of residual reactants after MSR. The other factor that can affect the temperature plots is the difference of temperature between moving balls and milling vial. This difference of temperature is arising from permanent motion of balls that prevent heat exchange due to point contacts between balls and vial. This temperature difference has been measured by Kwon et al. [29] in the range of 100–600 °C depending on milling conditions. Thus, it is expected that interrupting the mill let the balls to conduct their heat to the ambient. This phenomenon has been illustrated by Mehrabani and Babakhani [22]. By considering these heat sources we can explain the variations of temperature during mechanical milling. Accordingly the main heat source in the secondary temperature raise is gradual reaction of residual reactants. Additionally the heat generation by friction and collisions of balls is the other source in this step. The ΔT of ignition is a representation of the intensity of exothermic reaction. It was seen that by increasing the magnesium content, a greater amount of heat is released during MSR. Due to high temperature rise in MSR step, other heat sources are incapable of supplying needed heat to continue the increasing trend of the temperature quickly and consequently the temperature begins to drop. The outflow of heat from system (hot balls) interrupted the temperature drop after MSR peak and made a fairly horizontal line in the temperature variations plots for sample milled until MSR observation. After cooling of internal parts of milling system (balls and walls) the temperature dropped to the ambient temperature. The variations of temperature have been explained comprehensively by Mehrabani and Babakhani [22].

Fig. 9 shows the x-ray diffraction patterns of mixtures at various x values. It is seen that the peaks have become shorter until $x = 2$ but the overall composition has remained unchanged. The shortening of the peaks is due to refinement of particles and decrease of crystallinity. The composition of samples has been changed completely at x values more than 2. This is an indication of change in reaction mode (gradual to MSR) and confirm the time-

temperature plots. The intensity of diffraction patterns (in MSR mode) are increased by increasing magnesium content. As it can be seen the strongest peaks at $x = 2.5$ are W_2C and W respectively, while the W peaks are much stronger than W_2C at $x = 2.9$. Fig. 9 shows the normalized patterns to investigate the effect of composition on the milled product. Considering the shortening of peaks and crystal disordering, the illustration of phases with short peaks is difficult. Thus the unnormalized XRD patterns of important samples are shown in Fig. 10. $CaWO_4$ is the dominate phase at $x = 1.5$ and there is no new phase in the final powder. Investigations have shown nanoscale nucleation of products by solid-state diffusion of reactant atoms in the interface of particles. Researchers have used HRTEM and Raman spectroscopy techniques to detect these nuclei [35,36]. Accordingly similar events can occur in this sample but XRD is incapable for identification of these nuclei.

It is seen in Fig. 10 (at $x = 2$) that the WO_{3-x} and Ca_2MgWO_6 phases have appeared by increasing magnesium content. It should be noted that the reaction mode in this sample is gradual and the dominate phase is scheelite yet. Thus the reaction sequence of gradual mode can be explained as below:



Carbon needs long and severe milling to participate partially in gradual reactions due to thermodynamical conditions [37]. Therefore the absence of carbon containing compounds such as carbides in the patterns is normal.

As it is mentioned earlier, MSR occurs at $x \geq 2.5$ and hence the main phases of mixture change. Scheelite decreases and W_2C and W appear as dominate phases in this group of samples. The W_2C peaks are stronger than W peaks at $x = 2.5$, while W peaks become stronger by increasing magnesium content in the mixtures. Knowing the thermodynamic characteristics and stability temperature of these phases can be helpful to interpret the behavior of XRD patterns.

The best way for this purpose is the minimization of total Gibbs energy of system. This method determines the combination of n_i , P_i and X_i which minimizes the total Gibbs energy of the system. The

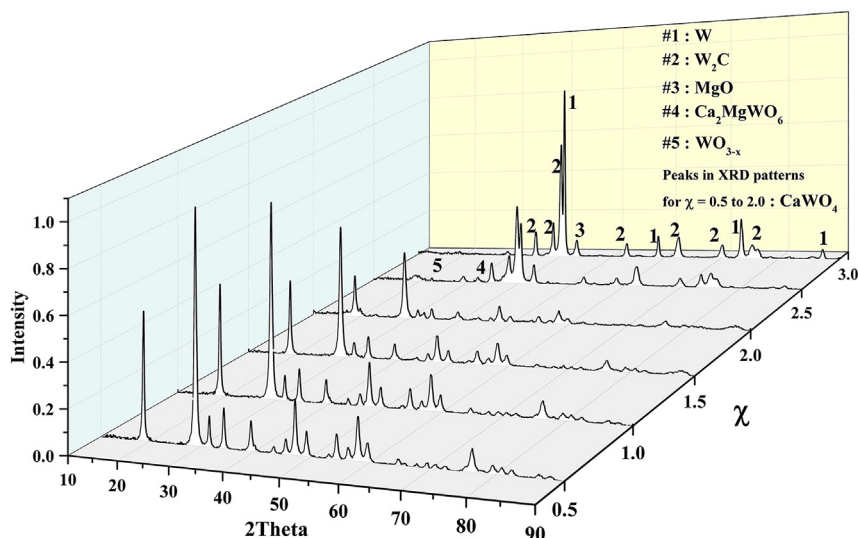


Fig. 9. X-ray diffraction patterns of samples at various x values.

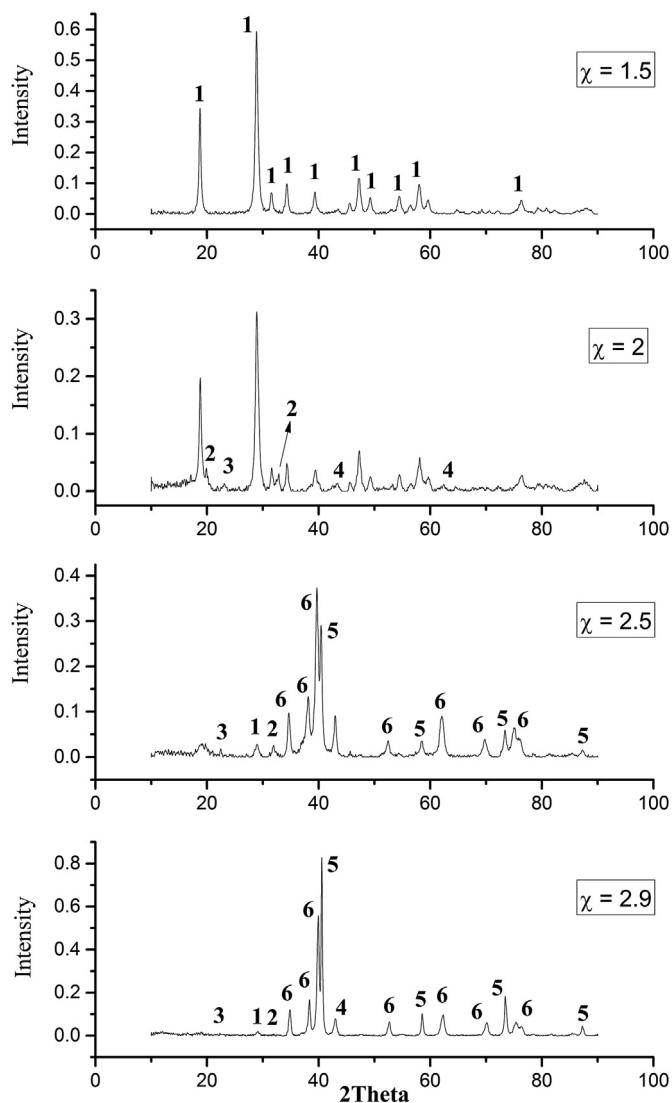


Fig. 10. Unnormalized XRD patterns of samples at various x values. The numbers indicate the phases as 1: CaWO_4 , 2: Ca_2MgWO_6 , 3: WO_{3-x} , 4: MgO , 5: W , 6: W_2C .

below equation represents the total Gibbs energy of the system:

$$\begin{aligned}
 G = & \sum_{\text{ideal}} n_i (g_i^\circ + RT \ln P_i) \\
 & + \sum_{\text{Pure}} n_i g_i^\circ \\
 & + \sum_{\text{Condensed Phases}} n_i (g_i^\circ + RT \ln X_i + RT \ln \gamma_i) \\
 & + \sum_{\text{Solution-1}} n_i (g_i^\circ + RT \ln X_i + RT \ln \gamma_i) \\
 & + \sum_{\text{Solution-2}} n_i (g_i^\circ + RT \ln X_i + RT \ln \gamma_i) \\
 & + \dots
 \end{aligned} \quad (11)$$

where n_i is the number of moles of species i , P_i is the partial pressure of species i , X_i is the mole fraction of species i , γ_i is the activity coefficient of species i and g_i° is the standard molar Gibbs energy of species i . Minimization of this equation at a constant temperature and pressure provides the equilibrium composition at the given conditions. A number of methods can be used to

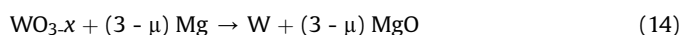
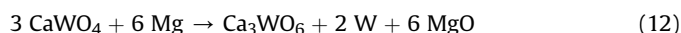
minimize the above equation but the Lagrange method is the common method for finding the minimum value of G . FactSage thermochemical software was used to calculate minimum value of G . The results are shown as a phase diagram in Fig. 11. This diagram was obtained by solving more than 1100 equations. The pressure and scheelite content were assumed constant in the calculations (1 atm). Only tungsten containing phases are shown to avoid a messy diagram. Black arrow on the horizontal axis shows the products of $\text{CaWO}_4\text{-Mg-C}$ mixture at $x = 3$. As it can be seen the stability of tungsten compounds by temperature increase can be considered as below:



As it was mentioned earlier, the adiabatic temperature increases by increasing magnesium content. Thus the formation of metallic tungsten is more preferred thermodynamically at higher x values. Therefore the tungsten peaks are stronger than W_2C at x values of 2.9 and 3. But the adiabatic temperature is lower at $x = 2.5$ and hence the W peaks are weaker than W_2C peaks. Due to lower adiabatic temperature the crystal structure is more disordered and consequently the intensity of XRD pattern is lower at $x = 2.5$ (Fig. 9).

WC forms in low temperatures and higher amounts of carbon content according to the Fig. 11, while it cannot be formed even at $x = 2.5$ practically. It is mentioned before that carbothermic reduction reaction of scheelite is activated by released heat of MSR. Thus a portion of carbon content are consumed in the carbothermic reduction reaction and hence due to carbon deficiency, W_2C forms instead of WC even at $x = 2.5$.

According to the XRD patterns and above mentioned events, reaction sequence of scheelite-magnesium-carbon mixtures in the MSR mode include two main steps. The first is reduction of scheelite and the second is formation tungsten carbides. Thus reaction sequence can be explained as below:



Then the MSR heat activates the endothermic reduction reaction of scheelite as below:



In the next step metallic tungsten reacts with carbon and W_2C forms as below:



Continued milling leads to the gradual conversion of W to W_2C . Fig. 12 shows the XRD patterns at $x = 3$. It can be seen that the tungsten peaks are weaker while W_2C peak become stronger by continuing milling process after MSR.

WC was not formed in the first group of experiments due to carbon deficiency and high adiabatic reaction. Accordingly the second group of experiments were carried out on $\text{CaWO}_4 - 3 \text{Mg} - (1 + y) \text{C}$ mixtures. Table 4 shows the reaction mode and CO evolution at various y values. As it can be seen CO gas was detected for samples in MSR mode. Fig. 13 shows the variations of t_{ig} and ΔT of ignition as a function of y value. It can be seen that addition of carbon increases ignition time. Ignition took place after 36 min of milling process at $y = 0$ while 84 min activation was needed for

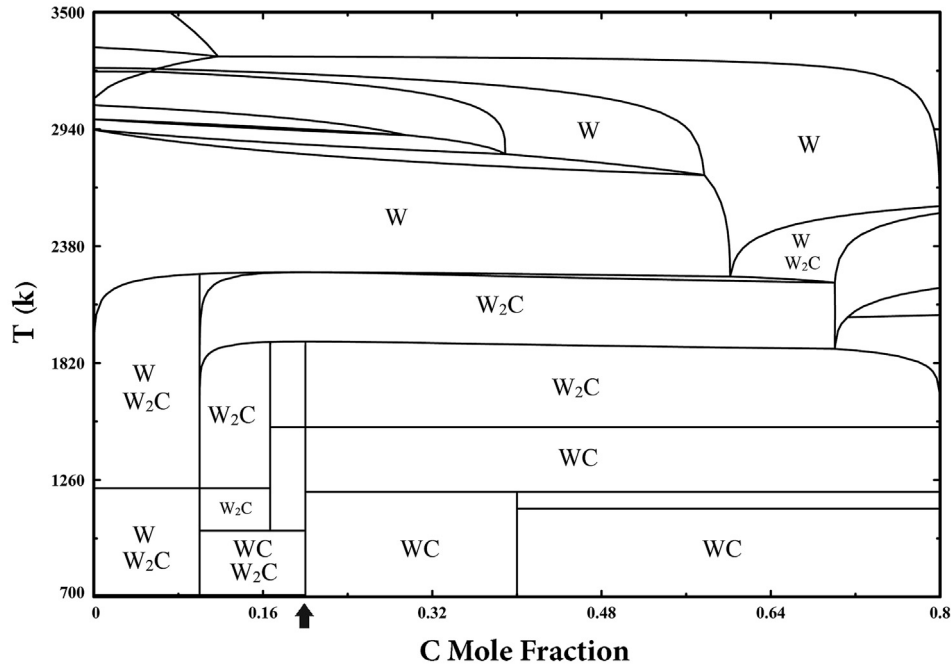


Fig. 11. $\text{CaWO}_4\text{-Mg-C}$ phase diagram, scheelite content is constant.

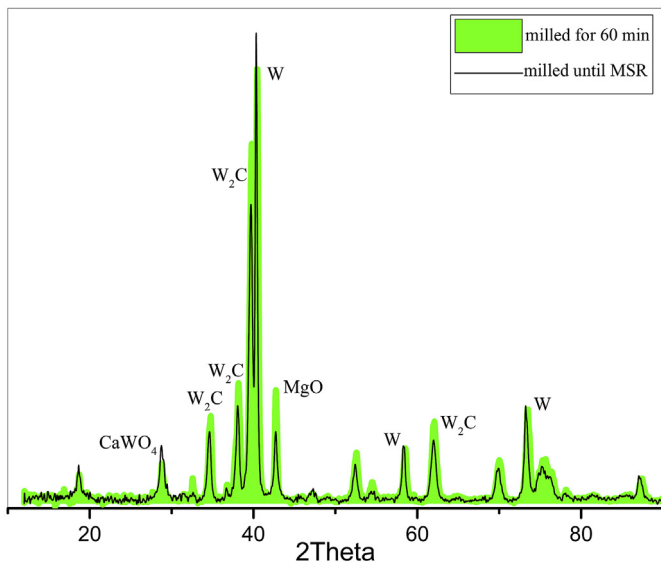


Fig. 12. XRD patterns of samples at $x = 3$ milled for 60 min and until MSR observation.

Table 4
Reaction mode and CO evolution at various y value.

y value	Reaction mode	CO gas
0–2.4	MSR	+
2.8	Gradual	–

occurrence of ignition at $y = 2.4$. The reaction mode was changed from MSR to gradual at $y = 2.8$. It has been discussed earlier that carbon cannot react with scheelite at low temperatures and thus acts as diluent before MSR process and prolong the ignition time. ΔT of ignition has an overall decreasing trend by increasing carbon content (Fig. 13). The temperature increased 3.5°C at $y = 0$ while

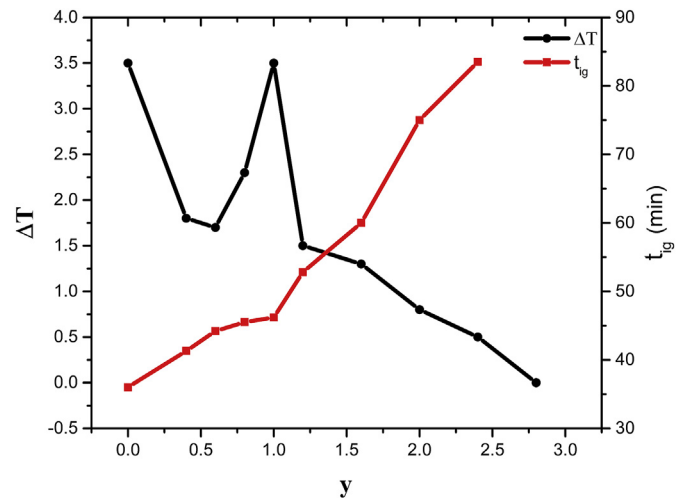


Fig. 13. Variations of ΔT of ignition and t_{ig} by y value.

there is only 0.5°C temperature raise at $y = 2.4$. The decreasing trend of ΔT of ignition is not uniform and there is two increase in the diagram. The first increase is at $y = 0.2$ and the second one is at $y = 0.8 - 1$. These tests were repeated several times to ensure the accuracy of the results. XRD was used to investigate the reason of these behaviors. Fig. 14 shows the XRD patterns of these samples.

As it can be seen in the patterns metallic tungsten is completely converted to W_2C in the range of 0–0.4. This is an exothermic reaction and could be the reason of the first increase in the ΔT of ignition diagram. Extra carbon absorbs the released heat at $y = 0.4$ and thus the ΔT of ignition decreases.

According to the XRD patterns WC is appeared in the range of 0.8–1 for the first time. Thus it can be concluded that the formation heat of WC increase the ΔT of ignition at y values between 0.8 and 1. This phase disappears again by increasing the carbon content in the mixture. Formation of tungsten carbides in W–C system at low

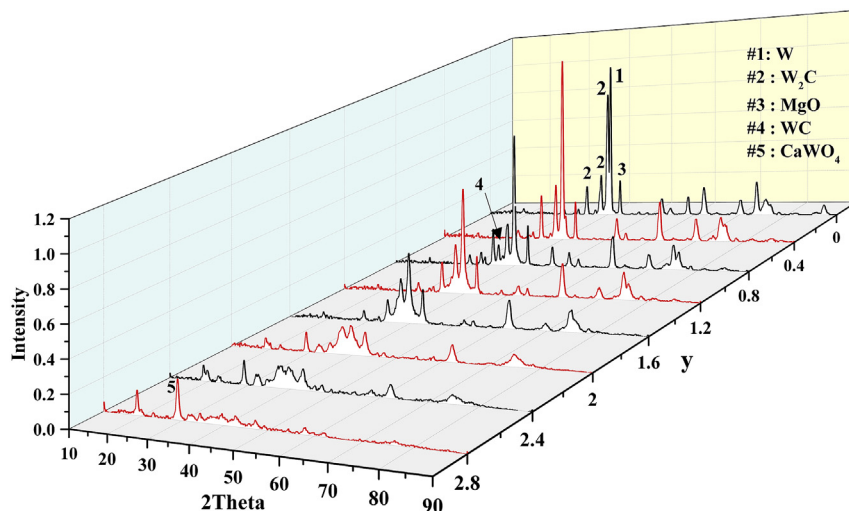


Fig. 14. XRD patterns of samples at various y values.

temperatures (1100 °C) has been investigated by Natter et al. [38]. They have reported that metallic tungsten was converted to W_2C in very short time (15 min). In addition WC was not formed until complete conversion of W to W_2C . The XRD patterns in Fig. 14 is in conformity with Natters investigations. It can be seen that WC was formed after complete conversion of W to W_2C . additionally it has been reported by Muhlbauer et al. [39] that the conversion of W_2C to WC is under control of diffusion and needs more time in comparison to the W_2C formation. Accordingly we can explain the disappearance of WC by increasing the carbon content. At $y = 0$ tungsten cannot convert to W_2C due to high adiabatic temperature and carbon deficiency. By increasing y value the adiabatic temperature decreases and the needed carbon for conversion of tungsten to W_2C is provided. But the temperature is too high for formation of WC. By increasing y value to 0.8–1, the conditions are provided for WC formation and thus this phase appears in the XRD patterns. Addition of more carbon decreases the temperature and thus the conversion of W_2C to WC, which is a diffusion - controlled reaction, gets interrupted and consequently this phase disappears again.

5. Conclusion

Fabrication of tungsten carbide via mechanically-induced self-propagating reaction (MSR) is the basic idea of this study. This process includes two steps. The first is the synthesis metallic tungsten and the second is formation of tungsten carbides. In the present study an aspect of the second step was investigated. The effect of magnesium and carbon contents on the products of MSR was described. It was seen that the metallic tungsten is more stable at higher temperatures and hence the tungsten peaks were stronger than W_2C peaks in samples with higher adiabatic temperature. It was seen that the released heat of exothermic reaction activate the carbothermic reduction of scheelite. On the other hand, calculations showed that formation of WC needs sufficient amount of carbon and low temperature. Thus, due to participation of carbon in reduction of scheelite, WC was not formed. In the second group of experiments, milling of $CaWO_4 - 3 Mg - (1 + y) C$ mixtures were investigated. The elimination of carbon deficiency was the aim of these experiments. It was seen that metallic tungsten was converted to W_2C . This reaction caused an increase in the ΔT of ignition. Addition of more carbon lead to the formation of WC at $y = 0.8 - 1$ which increased the ΔT of ignition. WC disappeared by

addition of more carbon due to decrease of adiabatic temperature and interruption of atomic diffusion.

Acknowledgment

This research was supported by Ferdowsi University of Mashhad, Iran under the Grant No. 3/42276.

References

- [1] Y. Gao, X. Song, X. Liu, C. Wei, H. Wang, G. Guo, On the formation of WC_{1-x} in nanocrystalline cemented carbides, *Scripta Mater.* 68 (2013) 108–110.
- [2] M. Razavi, M.R. Rahimpour, R. Yazdani-Rad, A novel technique for production of nano-crystalline mono tungsten carbide single phase via mechanical alloying, *J. Alloy. Comp.* 509 (2011) 6683–6688.
- [3] M.S. El-Eskandarany, Fabrication of nanocrystalline WC and nanocomposite WC–MgO refractory materials at room temperature, *J. Alloy. Comp.* 296 (2000) 175–182.
- [4] J. Ma, Y. Du, Synthesis of nanocrystalline hexagonal tungsten carbide via co-reduction of tungsten hexachloride and sodium carbonate with metallic magnesium, *J. Alloy. Comp.* 448 (2008) 215–218.
- [5] T. Ryu, H. Sohn, G. Han, Y.-U. Kim, K.S. Hwang, M. Mena, Z.Z. Fang, Nano-grained WC-Co composite powders by chemical vapor synthesis, *Metall. Mater. Trans. B* 39 (2008) 1–6.
- [6] E. Lassner, W.D. Schubert, Tungsten, Properties, Chemistry, Technology of the Element, Alloys, and Chemical Compounds, Kluwer Academic/Plenum Publishers, New York, USA, 1999.
- [7] T. Brown, P. Pitfield, Tungsten, *Critical Metals Handbook*, 2013, pp. 385–413.
- [8] A. Gupta, V. Singhal, O.P. Pandey, Facile in-situ synthesis of NbB₂ nanoparticles at low temperature, *J. Alloy. Comp.* 736 (2018) 306–313.
- [9] A. Gupta, M. Mittal, M.K. Singh, S.L. Suib, O.P. Pandey, Low temperature synthesis of NbC/C nano-composites as visible light photoactive catalyst, *Sci. Rep.* 8 (2018).
- [10] H. Singh, O.P. Pandey, A novel approach for direct synthesis of nanocrystalline tungsten carbide from milled scheelite ore, *Metall. Mater. Trans. B* 44 (2013) 1428–1434.
- [11] H. Singh, O.P. Pandey, Novel process for synthesis of nanocrystalline WC from wolframite ore, *Ceram. Int.* 41 (2015) 10481–10487.
- [12] R. Polini, E. Palmieri, G. Marcheselli, Effect of carbon excess and milling conditions on the synthesis of nanostructured WC by carbothermic reduction of scheelite ($CaWO_4$), *Int. J. Refract. Metals Hard Mater.* 54 (2016) 178–185.
- [13] R. Polini, E. Palmieri, G. Marcheselli, Nanostructured tungsten carbide synthesis by carbothermic reduction of scheelite: a comprehensive study, *Int. J. Refract. Metals Hard Mater.* 51 (2015) 289–300.
- [14] R. Polini, A. Marcucci, E. Palmieri, G. Marcheselli, Size tailoring of WC particles in the carbothermic reduction of scheelite ($CaWO_4$), *Int. J. Refract. Metals Hard Mater.* 64 (2017) 75–82.
- [15] H. Singh, O.P. Pandey, Effect of extended milling of scheelite ore with activated charcoal on direct synthesis of nanotungsten carbide, *Part. Sci. Technol.* 33 (2015) 587–592.
- [16] E.M. Pallone, D.R. Martin, R. Tomasi, W.J. Botta Filho, Al₂O₃–WC synthesis by high-energy reactive milling, *Mater. Sci. Eng., A* 464 (2007) 47–51.
- [17] M. Sakaki, M.S. Bafghi, J.V. Khaki, Q. Zhang, F. Saito, Control of carbon loss

- during synthesis of WC powder through ball milling of WO_3 -C-2Al mixture, *J. Alloy. Comp.* 486 (2009) 486–491.
- [18] M. Sakaki, M.S. Bafghi, J.V. Khaki, Q. Zhang, F. Saito, Conversion of W_2C to WC phase during mechano-chemical synthesis of nano-size WC- Al_2O_3 powder using WO_3 -2Al-(1+ x) C mixtures, *Int. J. Refract. Metals Hard Mater.* 36 (2013) 116–121.
- [19] M. Sakaki, M.S. Bafghi, J.V. Khaki, Q. Zhang, J. Kano, F. Saito, Effect of the aluminum content on the behavior of mechanochemical reactions in the WO_3 -C-Al system, *J. Alloy. Comp.* 480 (2009) 824–829.
- [20] M. Sakaki, M. Sh. Bafghi, J. Vahdati Khaki, Effect of heat absorbing alumina addition on mechanochemical synthesis of WC- Al_2O_3 nanocomposites, *Adv. Appl. Ceram.* 114 (2015) 144–149.
- [21] M.S. Bafghi, M. Sakaki, J.V. Khaki, Q. Zhang, F. Saito, Evaluation of process behavior and crystallite specifications of mechano-chemically synthesized WC-Al 2 O 3 nano-composites, *Mater. Res. Bull.* 49 (2014) 160–166.
- [22] H. yavari Mehrabani, A. Babakhani, An investigation on the mechanism and reaction sequence of scheelite-magnesium mixtures during mechanical milling, *Ceram. Int.* 44 (6) (2018) 6232–6241.
- [23] Dallas Semiconductor, Data Sheet for DS18B20 Programmable Resolution 1-Wire® Digital Thermometer, 2018. Technical report, <http://www.dalsemi.com>. Available at, <https://datasheets.maximintegrated.com/en/ds/DS18B20.pdf>.
- [24] Zhengzhou Winsen Electronics Technology Co, Technical Data MQ-7 Gas Sensor, Available at: <https://cdn.sparkfun.com/datasheets/Sensors/Biometric/MQ-7%20Ver1.3%20-%20Manual.pdf> 2014.
- [25] N. Novikov, I. Borovinskaya, in: A.G. Merzhanov, Chernogolovka (Eds.), *Combustion in Chemical Engineering and Metallurgy*, 1975, pp. 174–188. Moscow.
- [26] B. Lafuente, R.T. Downs, H. Yang, N. Stone, The Power of Databases: the RRUFF Project, *Highlights in Mineralogical Crystallography*, Walter de Gruyter GmbH 2016.
- [27] L.Y. Pustov, S.D. Kaloshkin, V.V. Tcherdyntsev, I.A. Tomilin, E.V. Shelekhov, A.I. Salimon, Experimental measurement and theoretical computation of milling intensity and temperature for the purpose of mechanical alloying kinetics description, *Mater. Sci. Forum* (2001) 373–378.
- [28] D.R. Maurice, T. Courtney, The physics of mechanical alloying: a first report, *Metal. Trans. A* 21 (1990) 289–303.
- [29] Y.-S. Kwon, K.B. Gerasimov, S.-K. Yoon, Ball temperatures during mechanical alloying in planetary mills, *J. Alloy. Comp.* 346 (2002) 276–281.
- [30] C. Suryanarayana, *Mechanical Alloying and Milling*, CRC Press, 2004.
- [31] H. Shalchian, J.V. Khaki, A. Babakhani, G. Taglieri, I. De Michelis, V. Daniele, F. Veglio, On the mechanism of molybdenite exfoliation during mechanical milling, *Ceram. Int.* 43 (2017) 12957–12967.
- [32] L. Takacs, Self-sustaining reactions induced by ball milling, *Prog. Mater. Sci.* 47 (2002) 355–414.
- [33] C. Deidda, S. Doppiu, M. Monagheddu, G. Cocco, A direct view of the self combustion behaviour of TiC system under milling, *J. Metastable Nanocryst. Mater.* (2003) 215–220. *Trans Tech Publ.*
- [34] C. Deidda, F. Delogu, G. Cocco, In situ characterisation of mechanically-induced self-propagating reactions, *J. Mater. Sci.* 39 (2004) 5315–5318.
- [35] J. Oghenevweta, D. Wexler, A. Calka, Early stages of phase formation before the ignition peak during mechanically induced self-propagating reactions (MSRs) of titanium and graphite, *Scripta Mater.* 122 (2016) 93–97.
- [36] J. Oghenevweta, D. Wexler, A. Calka, Sequence of phase evolution during mechanically induced self-propagating reaction synthesis of TiB and TiB 2 via magnetically controlled ball milling of titanium and boron powders, *J. Alloy. Comp.* 701 (2017) 380–391.
- [37] V.I. Stanciu, V. Vitry, F. Delaunois, Tungsten carbide powder obtained by direct carburization of tungsten trioxide using mechanical alloying method, *J. Alloy. Comp.* 659 (2016) 302–308.
- [38] H. Natter, A. Lackner, G. Knünz, R. Hempelmann, In Situ High Temperature X-ray Diffraction Study on Tungsten Carbide Formation, 2001.
- [39] G. Mühlbauer, G. Kremser, A. Bock, J. Weidow, W.-D. Schubert, Transition of W_2C to WC during carburization of tungsten metal powder, *Int. J. Refract. Metals Hard Mater.* 72 (2018) 141–148.